Catalysis Today 183 (2012) 88–95

Contents lists available at SciVerse ScienceDirect

Catalysis Today

journal homepage: www.elsevier.com/locate/cattod

A comparative study of Fe/SiO_2 Fischer–Tropsch synthesis catalysts using tetraethoxysilane and acidic silica sol as silica sources

Haiyun Suo[a,b,c,*], Chenghua Zhang[a,b,*], Baoshan Wu[a,b], Jian Xu[b], Yong Yang[a,b], Hongwei Xiang[a,b], Yongwang Li[a,b]

[a] State Key Laboratory of Coal Conversion, Institute of Coal Chemistry, Chinese Academy of Sciences, Taiyuan 030001, People's Republic of China
[b] National Engineering Laboratory for Indirect Coal Liquefaction, Institute of Coal Chemistry, Chinese Academy of Sciences, Taiyuan 030001, People's Republic of China
[c] Graduate University of Chinese Academy of Sciences, Beijing 10039, People's Republic of China

ARTICLE INFO

Article history:
Received 25 June 2011
Received in revised form 28 August 2011
Accepted 29 August 2011
Available online 25 September 2011

Keywords:
Fischer–Tropsch synthesis
Iron-based catalyst
Silica source
Tetraethoxysilane
Acidic silica sol

ABSTRACT

Fe/SiO_2 Fischer–Tropsch synthesis (FTS) catalysts using tetraethoxysilane (TEOS) and acidic silica sol (AcSS) respectively as silica sources were prepared by co-precipitation method. The catalysts were studied through N_2 adsorption, X-ray diffraction, Mössbauer effect spectroscopy, and temperature-programmed reduction and desorption. The FTS performances of catalysts were evaluated in a fixed-bed reactor at 280 °C, 1.5 MPa, 2000 h^{-1}, and H_2/CO molar ratio of 2. The characterization results indicated that the TEOS derived catalyst displayed a more uniform pore size distribution, easier reduction and higher capability for CO and H_2 adsorption than the AcSS derived catalyst. In FTS reactions, the TEOS derived catalyst showed higher activity and C_5^+ selectivity than the AcSS derived catalyst.

1. Introduction

Fischer–Tropsch synthesis (FTS) converting syngas into liquid fuels and chemicals is regarded as an important technology in coal, natural gas and biomass to liquid processes [1,2]. Iron based catalysts are preferred for FTS reaction due to their low cost, high activity and excellent water–gas–shift reactivity, which favor the conversion of syngas from coal gasification with low H_2/CO ratio [3].

In order to improve the FTS performance, structural promoters (especially SiO_2) are necessary additives in industrial iron-based catalysts [4,5]. The role of silica in FTS iron catalysts is generally considered to be physical in nature for providing large surface areas, stabilizing small iron crystallites and enhancing the attrition resistance of catalysts [6–8]. However, silica may also have significant effects on the catalyst activity and selectivity due to the metal–support interactions [9]. Dry and Oosthuizen [4] mentioned that the acidic oxides may react with basic alkali and thereby reduce the promotional effect of potassium in iron-based catalysts for FTS. Bukur et al. [5] and Yang et al. [10] observed an unexpected hydrocarbon distribution in $100Fe/5Cu/4.2K/xSiO_2$ catalysts and $100Fe/12Mn/1.5K/xSiO_2$ catalysts, respectively, i.e., the hydrocarbon spectrum tended to shift to higher molecular weight products when more amount of silica was added. In these studies, complicated interactions in multi-component FTS iron-based catalysts were observed. Especially, when chemical promoters were added, these promoters may affect the FTS performance individually or jointly [11]. Thus, complicated metal–support interactions usually have a synergetic effect on the FTS performance and make it difficult to explore the chemical function of silica in FTS iron-based catalysts. Some model catalysts were designed to study $Fe–SiO_2$ interactions in iron-based catalysts [9,12]. It was found in the reduction of Fe/SiO_2 catalyst that an iron (II) silicate phase may be formed, resulting in the inhabitation of the further reduction of iron oxides and the increase of light hydrocarbon selectivities in the FTS reaction. All these studies [5,9–12] indicated that silica has very important but complicated effects on FTS performances of iron-based catalysts. It is worthy of further investigation of the $Fe–SiO_2$ interaction on different aspects.

Although the Fe/SiO_2 catalysts for FTS have been extensively investigated, limited results have been reported for the effect of silica from different sources on iron-based catalysts. Acidic silica sol (AcSS) and tetraethoxysilane (TEOS) are widely used as silica sources in the preparation of Fe/SiO_2 catalysts [7,10]. They can be incorporated into catalysts during the precipitation of

* Corresponding authors at: State Key Laboratory of Coal Conversion, Institute of Coal Chemistry, Chinese Academy of Sciences, Taiyuan 030001, People's Republic of China. Tel.: +86 351 7117176; fax: +86 351 7560668.
E-mail addresses: suohaiyun1234@163.com (H. Suo), zhangchh@sxicc.ac.cn (C. Zhang).

0920-5861/$ – see front matter © 2011 Elsevier B.V. All rights reserved.
doi:10.1016/j.cattod.2011.08.047

catalyst precursors and have an obviously dispersive effect on the iron oxide phase. It is known that the TEOS is insoluble in aqueous solutions, but it can slowly hydrolyze to hydrophilic silica sol/gel. In the TEOS–water system, acids or bases can catalyze the hydrolysis of TEOS [13]. In contrast, acidic silica sol consists of amorphous silica colloid particles suspended in water [14]. In the process of the co-precipitation, TEOS hydrolyzes into silica accompanied by the precipitation of ferric ions, whereas the silica particles in AcSS may directly interact with ferric ions. Based on the different properties of two silica sources, varied structures may be formed and a diversity of physicochemical properties of catalysts are expected, such as morphology, dispersion, phases and so on. These differences may further affect the FTS activity and selectivity of catalysts. In this research, Fe/SiO_2 catalysts using TEOS and AcSS as silica sources were prepared by co-precipitation method. The catalysts were characterized by N_2 adsorption, H_2 temperature-programmed reduction (TPR), H_2 and CO temperature-programmed desorption (TPD), X-ray diffraction (XRD) and Mössbauer effect spectroscopy (MES). The FTS performance of catalysts was tested in a fixed-bed reactor and correlated with the characterization results.

2. Experimental

2.1. Catalyst preparation

Two model Fe/SiO_2 catalysts were prepared by co-precipitation method using TEOS and AcSS as silica sources, respectively. The detailed process of the co-precipitation method has been described elsewhere [10]. In brief, AcSS or alcoholic solution of TEOS was mixed with an aqueous solution of iron nitrate with a Fe/Si atomic ratio of 100/25. The mixed solution was precipitated using an ammonium solution at 80 °C and a pH value of 8.5–9.0. The obtained precipitate was aged for 2 h, and then washed and filtered afterwards. Then, the filtered cakes were dried at 120 °C overnight, followed by calcination at 500 °C for 5 h in air. The catalysts were denoted as Fe/SiO_2–TEOS and Fe/SiO_2–AcSS, respectively. Additionally, a pure Fe_2O_3 sample was used as a blank catalyst to compare the characterization results and FTS performance with Fe/SiO_2 catalysts.

2.2. Catalyst characterization

The BET surface area, pore volume and average pore diameter of fresh catalysts were measured by nitrogen physisorption at −196 °C in an ASAP 2420 (Micromeritics, USA). Each sample was degassed under vacuum at 90 °C for 1 h and 350 °C for 8 h prior to the measurement.

XRD patterns were obtained with a D/max-RA X-ray diffratometer (Rigaku, Japan), equipped with CuKα radiation (γ = 1.5406 Å) at 40 kV and 150 mA.

The Mössbauer effect spectroscopy (MES) experiments were carried out in a CANBERRA series 40 MCA constant-acceleration drive with a triangular reference signal at room temperature and/or −253 °C. The radioactive source was a 25 mCi ^{57}Co in Pd matrix. Data analysis was performed using a nonlinear least squares fitting routine that models the spectra as a combination of singlets, quadruple doublets, and magnetic sextets based on a Lorentzian line shape profile. The components were identified based on their isomer shift (IS), quadruple splitting (QS), and magnetic hyperfine field (Hhf).

H_2-TPR studies were carried out with an Autochem II 2920 equipment (Micromeritics, USA). 40 mg catalyst was loaded in a U-type quartz tube reactor and ramped from room temperature to 1000 °C in 10% H_2/90% Ar (mol/mol) at flow rate of 50 ml/min. The heating rate was maintained at 10 °C/min. The variation of the outlet gas concentration was monitored by a thermal conductivity detector (TCD). An isopropyl alcohol gel (−88 °C) was used to remove water formed during test. In order to quantify the degree of reduction in H_2-TPR, H_2 consumption amount of the reduction of stiochiometric CuO oxides was used as a calibration standard for peak areas under the same TPR procedure.

H_2-TPD studies were conducted in the same equipment as that of TPR. About 0.2 g of catalyst was placed in the reactor. The sample was reduced with pure H_2 (50 ml/min) at the temperature of 350 °C for 10 h. The catalyst was subsequently flushed at the same temperature with Ar for 30 min. After reduction, the sample was cooled to 50 °C and then H_2 flow continued for a period of 30 min at 50 °C. After adsorption, the system was purged with Ar flow (50 ml/min) to remove physisorbed H_2. The H_2-TPD profile was monitored using TCD when the temperature was increased at the rate of 10 °C/min from 50 °C to 800 °C.

CO-TPD experiments were performed in an atmospheric quartz tube flow reactor (5 mm i.d.). The outlet of the reactor was connected to a quadruple mass spectrometer through a capillary inlet system. In each CO-TPD experiment, 0.1 g of catalyst was loaded into the reactor and reduced with 5% CO/95% He (50 ml/min) at 300 °C for 12 h. Then the sample was cooled to 50 °C and switched to He until the baseline of CO signal leveled off. Finally, the temperature was increased to 800 °C at ramp of 10 °C/min. CO-TPD profiles were monitored by recording the mass signal of 28 in the outlet gas.

Table 1
Textural property of catalysts as-prepared.

Catalysts	BET surface area (m^2/g)	Pore volume (cm^3/g)	Average pore size (nm)
Fe_2O_3	18	0.17	32.2
Fe/SiO_2–TEOS	222	0.30	4.2
Fe/SiO_2–AcSS	218	0.50	7.7

2.3. Reactor system and operation procedure

The experiments were conducted in a 12 mm i.d. stainless steel tubular reactor. For all the experiments, 3 g catalysts (20–40 mesh) were loaded into the reactor, and the remaining volume of reactor was filled with quartz granules with the diameter of 10–20 and 20–40 mesh. The flow rates of gases were controlled by mass flow meters separately (5850E, Brooks), with the flow rate of the tail gas being measured by a wet-gas flow meter. All the catalysts were reduced with synthesis gas (H_2/CO = 2.0) at 300 °C and 1000 h^{-1} for 20 h. After the pretreatment, the reactor was cooled down to 220 °C and then the system was regulated to the reaction pressure (1.50 MPa) and weight hourly space velocity (2000 h^{-1}). The temperature was gradually increased to 280 °C at ramp of 10 °C/h. The TOS of all catalysts was about 200 h. The tail gas was analyzed on-line by gas chromatographs (GC) (models 6890N and 4890D; Agilent). The non-gaseous products in the hot and cold traps were collected over 24 h for the calculation of mass balance and sampled for analysis. After the reaction, passivation was done by introducing a flow of 1% O_2/99% N_2 at room temperature, and then the catalysts were collected and sealed in glass bottles for MES and XRD measurements.

3. Results and discussion

3.1. BET surface area

The BET surface area, pore volume and average pore diameter of catalysts are listed in Table 1. It can be seen that the BET surface area of the silica-free catalyst (Fe_2O_3) is about 18 m^2/g. Much

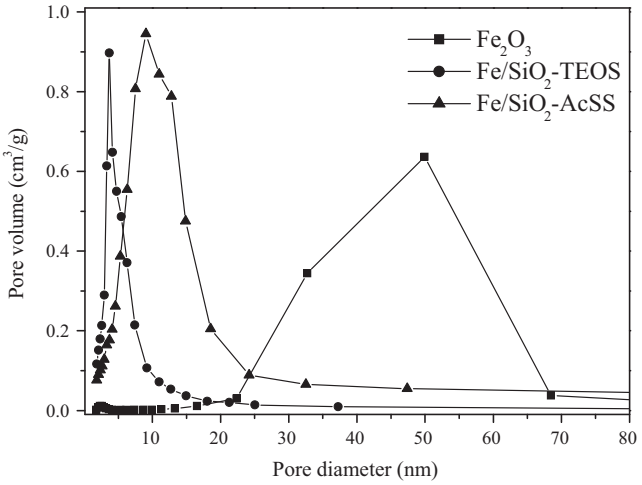

Fig. 1. The pore size distribution of catalysts as-prepared.

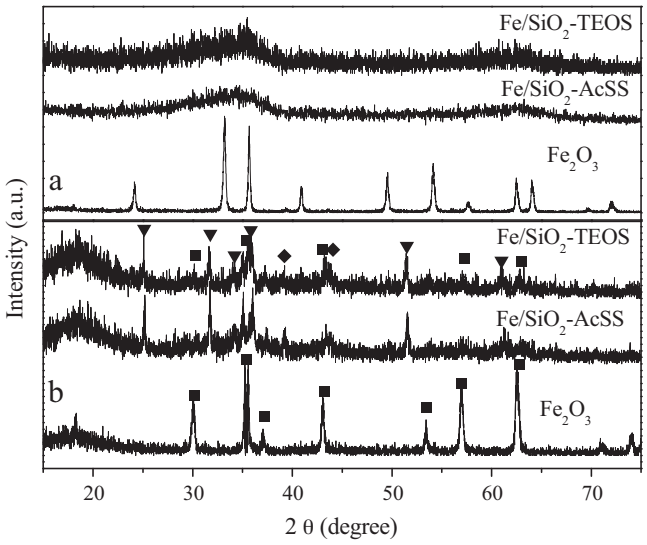

Fig. 2. XRD patterns of catalysts: (a) as-prepared; (b) after reaction; (■) magnetite; (♦) carbide; (▼) Fe_2SiO_4.

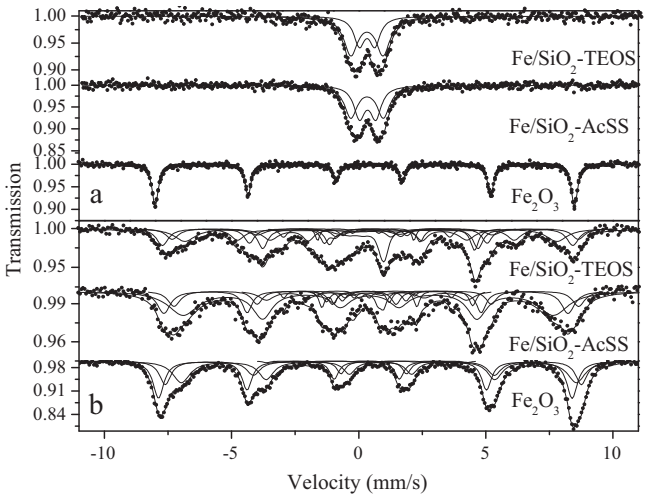

Fig. 3. Mössbauer spectra of catalysts: (a) as-prepared; (b) after reaction.

higher the BET surface area (about 220 m^2/g) and total pore volume are found for the catalysts containing SiO_2 compared with the silica-free catalyst (Fe_2O_3). In addition, the average pore diameter of the SiO_2-containing catalysts is smaller than that of Fe_2O_3. Although the SiO_2-containing catalysts have similar BET surface areas while the total pore volume and average pore diameter of the Fe/SiO_2–TEOS catalyst are smaller than those of the Fe/SiO_2–AcSS catalyst. The pore size distribution (PSD) in Fig. 1 shows that a larger pore diameter (20–70 nm) in the Fe_2O_3 catalyst. For the SiO_2-containing catalysts, the PSD curve shifts to smaller pore diameter compared with the Fe_2O_3 catalyst. It should be noted that the PSD curve of the Fe/SiO_2–AcSS catalyst is broad (2–25 nm) with a maximum at about 10 nm while the pore distribution curve of the Fe/SiO_2–TEOS catalyst is narrow (2–10 nm) with a maximum at about 4 nm. The results indicate that the pore distribution of the TEOS derived catalyst is much smaller and more uniform than those in the AcSS derived catalyst. In the preparation of the Fe/SiO_2–TEOS catalyst, the ferric ions were precipitated and accompanied by the TEOS hydrolysis. In contrast, the silica particles in AcSS may directly interact with ferric ions. The different properties of two silica sources may be lead to the different pore size distributions of two catalysts.

3.2. Crystalline structures of catalysts

XRD patterns of catalysts as-prepared are presented in Fig. 2a. It is obvious that iron phases in the Fe_2O_3 catalyst as-prepared are well-crystallized hematite with characteristic diffraction peaks at 2θ angle of 24.2°, 33.1°, 35.6°, 40.8°, 49.52°, 54.0°, 57.6°, 62.5° and 64.0°. In contrast, all the SiO_2-containing catalysts display broad diffraction peaks at 2θ values of 35° and 64°, which is the characteristic of amorphous iron oxides with small crystallite diameters [15]. This result implies that the crystallite size of iron oxide was reduced by the incorporation of SiO_2. Fig. 3a shows the Mössbauer spectra of catalysts as-prepared recorded at room temperature. The spectra parameters are given in Table 2. The MES spectra of the Fe_2O_3 catalyst is composed of one single sextet, which correspond to the paramagnetic α-Fe_2O_3 with particle size larger than 13.5 nm [16]. The Mössbauer patterns of both SiO_2-containing catalysts can be fitted into two doublets, which can be assigned to the Fe^{3+} superparamagnetic (spm) ions on the non-cubic sites with the crystallite diameters smaller than 13.5 nm [10,17]. It is known that the addition of SiO_2 improves the dispersion of iron oxide and prevents the aggregation of crystallites. XRD and MES results are in good agreement with the previous studies [10,12]. In addition, it can be found that doublets have similar isomer shift (IS) values but quite different quadrupole splitting (QS) values in both catalysts. Doublets with high QS values are attributed to spm Fe^{3+} ions on the surface while those with low QS values are attributed to spm Fe^{3+} ions in the bulk [18,19]. In the Fe/SiO_2–TEOS catalyst, the content of the surface Fe^{3+} ions is 65.9% while it is 54.2% in the Fe/SiO_2–AcSS catalyst. The results suggest that the TEOS derived silica has a better dispersion effect on the iron oxides than the AcSS derived one.

After FTS reactions, phase compositions of catalysts were determined by XRD and MES. The XRD patterns of the used catalysts are shown in Fig. 2b. It can be seen that the Fe_2O_3 catalyst only show diffraction peaks for Fe_3O_4 (JCPDS 85-1436) phase. For the SiO_2-containing catalysts, there are several diffraction peaks at 35.5°, 39.3°, 43.1°, 43.5°, 57.0° and 62.6°. The peaks at 35.5°, 43.1°, 57.0° and 62.6° are attributed to the characteristic diffraction of Fe_3O_4. The peaks at 39.3°, 43.4° and 43.5° are attributed to the characteristic diffraction of iron carbides (Fe_5C_2). Additionally, the characteristic peaks of Fe_2SiO_4 (JCPDS 76-0512) are observed at 2θ values of 35°, 25.1°, 31.6°, 36.0°, 37.3°, 51.4° and 61.0° for two catalysts. According to literatures [9,20], iron (II) silicate was formed during the initial stage of reduction, which cannot be reduced completely even at high temperature. This result indicates that

Table 2
Mössbauer parameters of catalysts.

Catalysts	Phases	Mössbauer parameters			
		IS (mm/s)	QS (mm/s)	Hhf (kOe)	Area (%)
As-prepared[a]					
Fe_2O_3	α-Fe_2O_3	0.36	−0.21	513	100.0
Fe/SiO_2–TEOS	Fe^{3+} (spm in surface)	0.33	1.27		64.9
	Fe^{3+} (spm in bulk)	0.33	0.61		35.1
Fe/SiO_2–AcSS	Fe^{3+} (spm in surface)	0.33	1.25		54.2
	Fe^{3+} (spm in bulk)	0.35	0.64		45.8
After reaction[b]					
Fe_2O_3	Fe_3O_4	0.29	−0.04	506	37.3
		0.59	−0.02	509	25.2
		0.82	−0.04	483	35.2
	χ-Fe_5C_2	0.30	0.03	245	1.2
		0.30	0.02	207	1.1
Fe/SiO_2–TEOS	Fe_3O_4	0.36	−0.03	502	16.0
		0.65	0.01	497	10.7
		0.47	0.02	455	21.1
		0.67	0.02	338	12.0
	χ-Fe_5C_2	0.32	0.13	240	13.9
		0.29	0.04	203	5.4
		0.35	0.35	117	7.6
	Fe_2SiO_4	1.33	2.93	110	13.3
Fe/SiO_2–AcSS	Fe_3O_4	0.25	0.07	496	18.8
		0.65	0.08	495	12.3
		0.40	−0.06	453	46.8
	χ-Fe_5C_2	0.30	0.01	245	7.8
		0.32	0.06	205	2.4
		0.27	0.30	116	5.6
	Fe_2SiO_4	1.26	2.98	109	6.3

[a] The catalysts as-prepared were measured at room temperature.
[b] The catalysts after reaction were measured at −253 °C.

a strong Fe–SiO_2 interaction apparently exists in both Fe/SiO_2 catalysts. In order to further determine iron phase compositions of catalysts, used catalysts were measured by MES at −253 °C. The spectra (Fig. 3b) exhibited complex magnetic interactions due to the presence of multiple magnetic phases. MES parameters of various phases and their relative contributions to spectral absorption areas are tabulated in Table 2. As shown in Fig. 3b, all Mössbauer patterns can be fitted with five or six sextets. The subspectra with Hhf in the range of 490–510 kOe are contributed to the Fe^{3+} sites while those with Hhf in the range of 300–480 kOe are contributed to the Fe^{2+} sites of ferrimagnetic Fe_3O_4 phases [21,22]. The subspectra with 0.20 mm/s < IS <0.40 mm/s and 110 kOe < Hhf <250 kOe correspond to the three different sites of stiochiometric iron carbide (χ-Fe_5C_2) [23,24]. In addition, the sub-spectrum with IS = 1.33 mm/s and QS = 2.93 mm/s is associated with crystalline (Fe_2SiO_4) [25]. The MES results indicate that the main phase of SiO_2-free sample (Fe_2O_3) is Fe_3O_4 (97.7%), which is in agreement with XRD results. The MES spectrum of the SiO_2-containing catalysts was fitted in the same way. It can be clearly seen that both Fe/SiO_2 catalysts are composed of magnetite, iron carbide and Fe_2SiO_4. However, in the SiO_2-containing catalysts, the content of iron carbide is higher than that of Fe_2O_3 sample. Under typical FTS conditions where H_2O is present, the iron carbides can be oxidized to Fe_3O_4 [26], especially for the unsupported iron catalyst [27]. As reported in literature [10], SiO_2 could stabilize the iron carbides due to the Fe–SiO_2 interaction, which is in agreement with present results. However, in Fe/SiO_2–TEOS catalyst, contents of iron carbide and Fe_2SiO_4 are higher than those in Fe/SiO_2–AcSS catalyst. The high iron carbide content indicates that the TEOS derived catalyst can be easily reduced into active carbide phases in FTS reaction. Similarly, the high Fe_2SiO_4 content also implies that more iron species interact directly with TEOS derived silica in Fe/SiO_2–TEOS catalyst. Although the strong Fe–SiO_2 interaction leads to more inactive Fe_2SiO_4 phases, the Fe/SiO_2–TEOS catalyst seems to become easier for the formation of active phases. This phenomenon is probably caused by the high dispersion of TEOS derived silica. High dispersed silica has high contacting interfaces with iron species. Simultaneously, the dispersion effect also leads to abundant exposures of iron oxides not directly adjacent to silica, which favor the activation of this part of iron oxides.

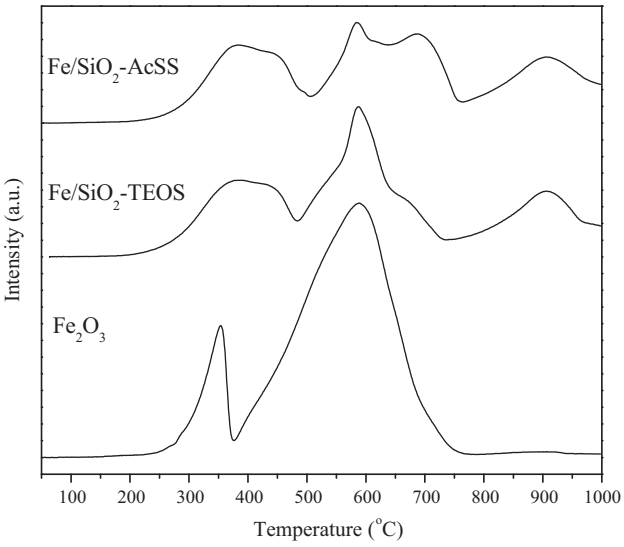

Fig. 4. H_2-TPR profiles of catalysts.

3.3. Reduction behaviors of catalysts

Reduction behaviors of catalysts were investigated by H_2-TPR. H_2-TPR profiles of catalysts are shown in Fig. 4 and H_2 consumptions at different stages are listed in Table 3. As shown in the figure, the profile of Fe_2O_3 catalyst shows two well-separated H_2 consumption peaks at about 377 °C and 589 °C, corresponding to the

Table 3
Quantitative results of H_2 consumption in H_2-TPR process.

Catalysts	Peak (°C)	H_2 consumption (mol H_2/mol Fe)	Total H_2 consumption (mol H_2/mol Fe)
Fe_2O_3	354	0.17	1.49
	589	1.32	
Fe/SiO_2–TEOS	390	0.46	1.37
	588	0.45	
	655	0.09	
	906	0.37	
Fe/SiO_2–AcSS	390	0.43	1.36
	589	0.25	
	690	0.28	
	904	0.40	

reduction of α-Fe_2O_3 to Fe_3O_4 and Fe_3O_4 to α-Fe [27], respectively. It is clear that silica incorporation significantly affects the reduction behavior of the iron catalyst. The TPR profile of Fe/SiO_2–AcSS catalyst shows four reduction peaks at about 390, 589, 690 and 904 °C, which can be assigned to three different reduction stages of iron oxides. The hydrogen consumption for the first peak (390 °C) is 0.43 mol H_2/mol Fe, which is considerably higher than the theoretical H_2 consumption for the reduction of Fe_2O_3 to Fe_3O_4 (0.17 mol H_2/mol Fe), and which is lower than the theoretical value for the reduction of Fe_2O_3 to Fe^{2+} species (0.5 mol H_2/mol Fe). Therefore, the first peak can be attributed to the reduction of α-Fe_2O_3 to Fe_3O_4 and part of Fe_3O_4 to Fe^{2+} species [28]. Correspondingly, the second peak (589 °C) and the third peak (690 °C) can be assigned to the reduction of Fe_3O_4 and Fe^{2+} species to α-Fe. In the case of silica-contained iron catalysts, it has been reported that iron (II) silicate [12,20] may form during the reduction and hinder the further reduction of these iron species to metallic iron. In our study, the Fe_2SiO_4 phase can also be detected by XRD and MES after reaction. Thus, the reduction peak above 900 °C can be ascribed to the reduction of iron oxide species that strongly interact with silica (very likely present as Fe_2SiO_4 species). In the TPR profile of the Fe/SiO_2–TEOS catalyst, there are also four reduction peaks. Compared to the Fe/SiO_2–AcSS catalyst, the peak positions and the hydrogen consumptions of the first and the fourth peaks hardly vary. It indicates that the first and the last reduction stages for both catalysts are similar to each other. Previous studies [10,28,29] have proposed that a strong interaction between Fe crystallites and the SiO_2 matrix was formed in iron catalysts incorporated with SiO_2. This interaction can stabilize Fe^{2+} species as the intermediate phase and restrain its further reduction to α-Fe. In present study, Fe^{2+} species (likely present as FeO and Fe_2SiO_4 species) also formed during the reduction process, which indicates that a strong metal–silica interaction apparently exists in both silica incorporated catalysts. In addition, total hydrogen consumptions for both Fe/SiO_2 catalysts are lower than those of Fe_2O_3 catalyst (1.49 mol H_2/mol Fe). Apparently, these catalysts are not completely reduced in H_2 atmosphere below 1000 °C. This result further demonstrates that the strong Fe–SiO_2 interaction inhibits the reduction of iron oxides. Nevertheless, in Fe/SiO_2–TEOS catalyst, the hydrogen consumption for the second peak (588 °C) is intensified, and the third peak (655 °C) is obviously reduced relative to the Fe/SiO_2–AcSS catalyst. This result indicates that the reduction of Fe/SiO_2–TEOS catalyst in the second stage becomes easier probably due to the higher dispersion effect of TEOS derived silica as confirmed by BET and MES results. In previous works [30], supported iron catalysts are difficult to be reduced. It is possibly resulted from high dispersion states of iron oxides, which have larger proportions of interface atoms with the support. However, those supported catalysts contain low iron contents than co-precipitated catalysts in our study. Therefore, silica in present catalysts is not high enough to interact with all iron species. Only part of iron species directly contact with SiO_2 to form hardly reducible iron species, such as iron (II) silicate. The rest of iron species not directly adjacent to silica would remain as iron oxides with different dispersions. The reduction of this part of iron species would be improved by the dispersion effect of silica because higher dispersion leads to larger percentages of exposed surface atoms and higher contacting probability of these atoms with H_2 during the reduction. Undoubtedly, the highly dispersed Fe/SiO_2–TEOS catalyst has a better reduction behavior than Fe/SiO_2–AcSS catalyst in the second reduction stage.

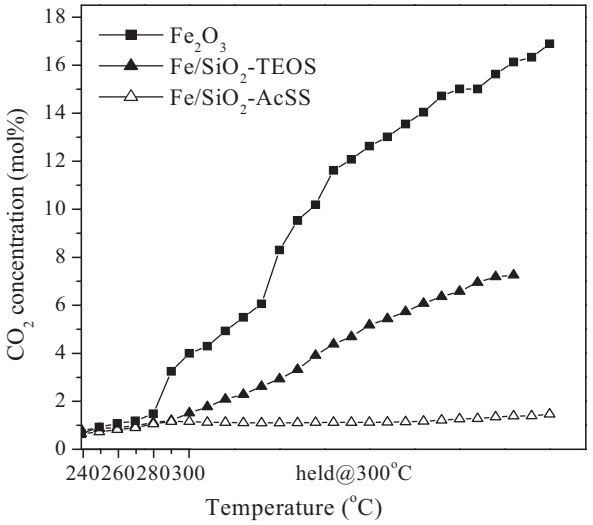

Fig. 5. In situ reduction behaviors of catalysts in syngas.

Activation behaviors of catalysts in syngas are shown in Fig. 5 as the change of CO_2 concentration in the tail gas during the in situ pretreatment, which can monitor the reduction degree of the catalysts or the formation of FTS active phases. With increasing reduction temperature to 300 °C, the CO_2 concentration of the Fe_2O_3 catalyst rapidly increases to a much high level (ca. 16.9%). However, the CO_2 concentrations of both SiO_2-containing catalysts show a slow and gradual ascending tendency at the low concentration level, which suggests the inhibitive effect of SiO_2 on the reduction of catalysts in syngas. In addition, it can be found that the CO_2 concentration of Fe/SiO_2–TEOS is apparently higher than that of Fe/SiO_2–AcSS during the whole reduction process. It is consistent with the result of H_2-TPR which indicates a higher reduction extent for Fe/SiO_2–TEOS catalyst than that for Fe/SiO_2–AcSS catalyst.

3.4. Adsorption behaviors of catalysts

H_2-TPD is used to investigate H_2 chemisorption behavior of catalysts shown in Fig. 6. From the figure, the H_2 desorption over silica-free catalyst (Fe_2O_3) mainly occurs at two temperature ranges: a sharp peak at ca. 70–100 °C and broad tail at 120–300 °C. However, it can be found in the figure that four H_2 desorption peaks are distinct on H_2-TPD profiles of both Fe/SiO_2 catalysts. These peaks could be assigned to four different adsorption states on the catalyst surface: desorbing at 80–100 °C (H_α), desorbing at about 180–280 °C (H_β), desorbing at 430 °C (H_γ) and desorbing at 540 °C (H_δ). As reported in literature [31,32], two adsorption states (at about 20–80 and 100–180 °C) were observed for Fe (1 0 0) surface. Weatherbee et al. [33] found that H_2 thermal desorption peaks on polycrystalline iron occurred at around 0–300 °C regions. The H_2-TPD profile of Fe_2O_3 sample and low temperature desorption peaks (below 300 °C) in Fe/SiO_2 catalysts are similar to above literature results. Therefore, the H_α and H_β species could be ascribed to hydrogen chemisorbed weakly and strongly on the metallic iron sites, respectively. In present study, H_2-TPD spectra

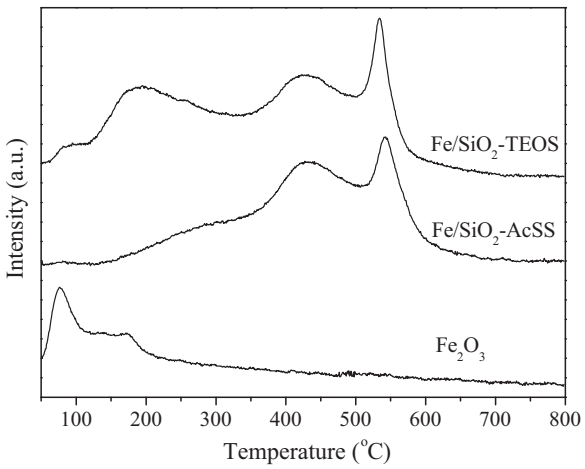

Fig. 6. H_2-TPD profiles of catalysts.

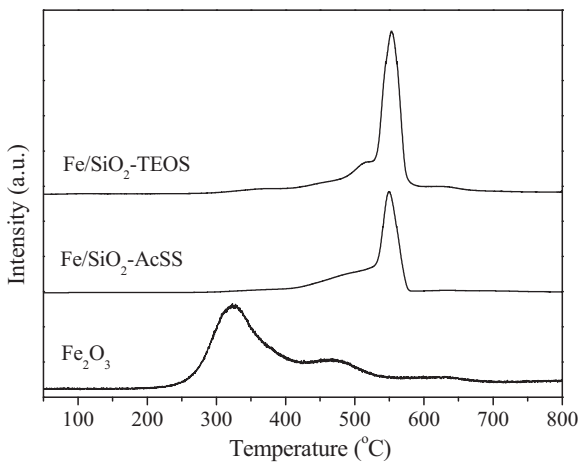

Fig. 7. CO-TPD profiles of catalysts.

of Fe/SiO_2 catalysts are quite different compared to the present Fe_2O_3 catalyst and those observed previously for single crystal and polycrystalline iron [31–33]. It is evident that the adsorption of hydrogen did not occur at high temperature regions (above 300 °C) for those catalysts. In supported metal catalysts [34,35], H_2 desorption peaks at higher temperature regions were observed and attributed to H_2 evolved from very strong chemisorption sites on the metal–support interface and the support as spilt-over species due to metal–support interaction. According to literatures [33,36], the chemisorption of H_2 on iron is sensitive to perturbation of the electronic and/or surface geometric structure caused by metal–support or metal–promoter interactions. In this study, both SiO_2-containing catalysts show a strong Fe–SiO_2 interaction and lead to the formation of hardly reducible iron oxides during reduction process. In addition, Clausen et al. [37] also revealed that H_2 could chemisorb on non-metallic forms of iron in the case of silica supported iron-based catalyst. Therefore, desorption peaks at high temperature regions (H_γ and H_δ) may be attributed to hydrogen chemisorbed on the unreduced iron oxide and/or iron silicate compounds of catalysts. Apparently, desorption peaks for H_γ and H_δ species are very similar on both catalysts, which is in good agreement with the identical silica content and similar strong Fe–SiO_2 interactions in both catalysts. However, desorption peaks of H_α and H_β species on the Fe/SiO_2–TEOS catalyst are much higher than those on the Fe/SiO_2–AcSS catalyst, which indicates that the highly dispersed Fe/SiO_2–TEOS catalyst has more hydrogen adsorption sites. In addition, H_2-TPR and tail gas analysis revealed that the reducibility of Fe/SiO_2–TEOS catalyst was higher than that of Fe/SiO_2–AcSS catalyst. Consequently, more metallic iron sites could be formed on the Fe/SiO_2–TEOS catalyst in the process of pretreatment.

CO-TPD curves of CO-carburized catalysts are shown in Fig. 7. As can be seen, the CO desorption profile of the Fe_2O_3 catalyst demonstrates a sharp peak at 325 °C and a small peak at 469 °C. Nevertheless, CO desorption curves for both Fe/SiO_2 catalysts shift to high temperatures, exhibiting a broad peak at around 510 °C and a sharp peak at 550 °C. It is indicated that silica apparent influences the CO adsorptions on carburized catalyst surfaces. It was reported that the desorption temperature of molecular CO adsorbed on metallic iron surface is always below 200 °C, and desorption peaks above 300 °C usually result from desorption of dissociated CO [38,39]. In this work, no obvious CO adsorption species was desorbed below 300 °C for all catalysts. The desorption temperatures of CO on carburized catalysts are far higher than those of the molecular CO on the single crystal iron surface and close to that of the dissociative CO [38–40]. Therefore, all CO desorption peaks can be ascribed to the recombination of surface dissociated carbon and oxygen atoms. It is worthy of noting that the CO-TPD peak of Fe/SiO_2–TEOS catalyst is apparently higher in intensity than that of Fe/SiO_2–AcSS catalyst, which indicates that the Fe/SiO_2–TEOS catalyst has more CO adsorption sites than the Fe/SiO_2–AcSS catalyst.

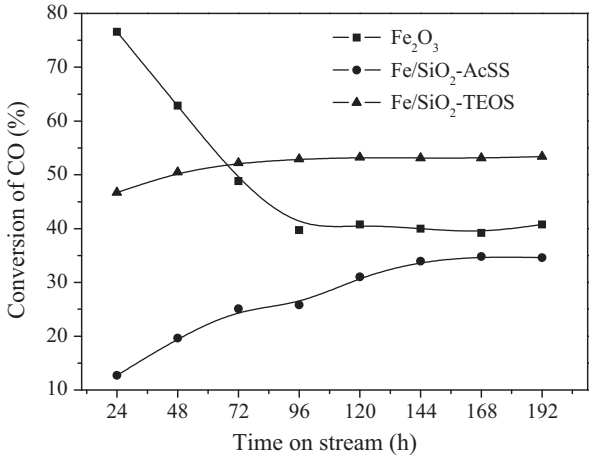

Fig. 8. The carbon monoxide conversion with time on stream for all catalysts.

3.5. FTS performance

FTS activities of catalysts with time on stream (TOS) are shown in Fig. 8. Specific activities and selectivities of catalysts at TOS of 96 and 192 h are summarized in Table 4. There is an apparent deactivation phenomenon for Fe_2O_3 catalyst, i.e. the CO conversion is at a high level (77%) at the beginning of the reaction, and rapidly decreases from 77% at 24 h on stream to about 40% at 96 h on stream. In the case of the Fe/SiO_2–AcSS catalyst, the CO conversion is initially lower than 13% and gradually increases to about 35% after a period of 200 h. This increase in the catalytic activity may be caused by the further reduction and carburization of the catalyst during FTS run [11]. For the Fe/SiO_2–TEOS catalyst, the initial CO conversion is 47%. It further increases to about 53% after a period of 100 h, and maintains stable thereafter. It is evident that initial CO conversions of SiO_2-containing catalysts are lower but better in stability than that of Fe_2O_3 catalyst. It is known that the Fe–SiO_2 interactions suppress the reduction and carburization of iron oxides and decrease the reaction activity. At the same time, silica has stabilizing effects on FTS performances of iron-based catalysts, which

Table 4
Activities and selectivities of catalysts.

Catalysts[a]	Fe/SiO_2–TEOS		Fe/SiO_2–AcSS		Fe_2O_3	
Time on stream (h)	96	192	96	192	96	192
CO conversion (%)	52.9	53.4	25.8	34.6	39.7	40.8
CO + H_2 conversion (%)	46.7	47.4	23.9	33.2	34.0	35.7
H_2 conversion (%)	43.5	44.4	22.9	32.5	30.9	33.1
H_2/CO (in tail gas)	2.36	2.43	2.04	2.10	2.16	2.13
H_2/CO usage	1.62	1.69	1.74	1.92	1.46	1.53
CO STY[b] ($mmol/g_{cat}/h$)	16.0	15.8	7.8	10.2	12.4	12.7
H_2 STY ($mmol/g_{cat}/h$)	25.9	26.7	13.6	19.6	18.1	19.4
CO_2 STY ($mmol/g_{cat}/h$)	2.9	2.9	1.0	1.5	2.8	2.9
HC[c] STY ($mg/g_{cat}/h$)	175.4	171.0	90.6	116.4	140.4	144.0
$Kp = P_{CO2}P_{H2}/P_{CO}/P_{H2O}$	0.68	0.68	0.34	0.48	0.83	0.85
HC[c] selectivity (wt%)						
C_1	15.2	16.9	22.1	22.0	22.7	23.6
C_2–C_4	39.5	41.1	45.2	44.1	47.3	44.5
C_5^+	45.3	42.0	32.7	33.9	30.0	31.9
$C_{2-4}^{=}/C_{2-4}^{0}$	0.48	0.46	0.35	0.36	0.43	0.40
$C_{5-11}^{=}/C_{5-11}^{0}$	0.44	0.44	0.41	0.41	0.42	0.43

[a] Reaction conditions: 280 °C, 1.5 MPa, $H_2/CO = 2.0$, 2000 h^{-1}.
[b] Space-time-yield.
[c] Hydrocarbon.

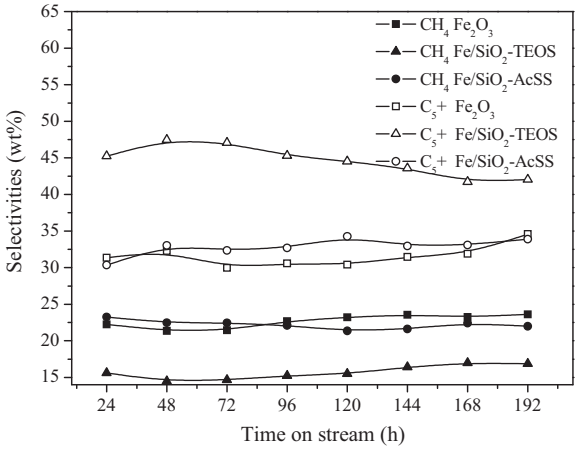

Fig. 9. The selectivity with time on stream for all catalysts.

has been reported in many works [10,12,41]. It is worthy of noting that the TEOS derived silica apparently improves the stability with a less activity loss in FTS reaction. Two main factors may be associated with the improvement. Firstly, as is indicated by MES measurement (Fig. 3a), the dispersion of iron oxide particles is higher in the TEOS derived catalyst. A larger amount of surface active sites would be expected to form in the FTS reaction. This has been verified by the TPD results. More CO and H_2 are adsorbed on the Fe/SiO_2–TEOS catalyst. Therefore, it is reasonable for the high CO conversion activity of the TEOS derived catalyst. Secondly, H_2-TPR and tail gas analysis during reduction process revealed that the reduction of Fe/SiO_2–TEOS catalyst is easier than that of Fe/SiO_2–AcSS catalyst. Therefore, more active carbide species can be formed in the Fe/SiO_2–TEOS catalyst during the FTS process. MES results of the used catalysts also confirmed that the Fe/SiO_2–TEOS catalyst has a higher content of iron carbides than the Fe/SiO_2–AcSS catalyst.

FTS selectivities of catalysts with time on stream (TOS) are shown in Fig. 9. It can be found that Fe_2O_3 and Fe/SiO_2–AcSS have similar hydrocarbon product distributions. However, the CH_4 selectivity of Fe/SiO_2–TEOS catalyst is about 15 wt%, which is apparently lower than that of Fe/SiO_2–AcSS catalyst (about 22 wt%). The C_5^+ selectivity of the Fe/SiO_2–TEOS (about 44 wt%) is higher than that of Fe/SiO_2–AcSS (about 34 wt%). Olefin selectivities of the Fe/SiO_2–TEOS catalyst including and C_2–C_4 and C_5–C_{11} are slightly higher than those of Fe/SiO_2–AcSS catalyst. Obviously, the Fe/SiO_2–TEOS catalyst suppresses the selectivity to methane and enhances the selectivities to olefins and C_5^+ hydrocarbons.

The H_2/CO ratio has a great effect on the product selectivity. It is widely accepted that low H_2/CO ratio would facilitate the chain growth reaction on the iron catalyst [11]. However, Table 4 shows that a H_2/CO exit ratio of the Fe/SiO_2–AcSS catalyst is lower than that of the Fe/SiO_2–TEOS catalyst due to the relative low CO conversion of the Fe/SiO_2–AcSS catalyst. Therefore, the effect of H_2/CO ratio can be withdrawn. Zhang et al. [12] found that the SiO_2-contained iron catalyst leads to a poor reducibility and an enhancement in the light hydrocarbon selectivity. Similarly, our results indicate that the Fe/SiO_2–AcSS catalyst has lower reduction degree than the Fe/SiO_2–TEOS catalyst in syngas pretreatment. Therefore, more iron oxide phases in terms of Fe_3O_4 or Fe^{2+} species should exist in the Fe/SiO_2–AcSS catalyst. Surface oxygen can inhibit the adsorption of H_2 and CO on transition metal surfaces, especially for the CO dissociation [38]. Hence, the variation of surface adsorbed C and H species may change the chain growth probability and the formation of heavy hydrocarbons. On the other hand, the dispersion degree of the active phases in the catalyst also has some impact on the hydrocarbon distribution. Some researchers [42,43] reported that the methane formation was inhibited on highly dispersed iron catalysts. In the Fe/SiO_2–TEOS catalyst, the dispersion effect of silica can increase the proportion of surface active iron sites and decrease the coordination number of surface active iron sites. These coordinately unsaturated iron active sites have a tendency to interact strongly with adsorbate species (C, H). Stronger Fe–C and Fe–H bonds are not favorable for the hydrogenation of surface C species to methane [44]. As a synergistic effect of factors mentioned above, the Fe/SiO_2–TEOS catalyst shows lower methane and higher C_5^+ selectivities than the Fe/SiO_2–AcSS catalyst.

4. Conclusions

Both silica sources of TEOS and AcSS can provide more than 200 m^2/g surface areas for Fe/SiO_2 catalysts. The catalyst using TEOS as the silica source has more uniform pore size distribution and higher dispersion of iron oxides than that using AcSS as the silica source. The TEOS derived catalyst has a higher degree of reduction and/or carburization in H_2 or syngas. Moreover, more adsorption sites for H_2 and CO are formed on the surface of the TEOS derived catalyst. After reactions, both catalysts have similar iron

phase structures while the Fe/SiO_2–TEOS catalyst contains more iron carbide than the Fe/SiO_2–AcSS catalyst. Thus, the Fe/SiO_2–TEOS catalyst exhibits a high activity in FTS reaction. Additionally, the methane formation is inhibited on the Fe/SiO_2–TEOS catalyst probably due to higher dispersion of active phases (iron carbides) and less inactive phase (iron oxides).

Acknowledgements

Financial supports from the National Outstanding Young Scientists Foundation of China (20625620) and the National Natural Science Foundation of China (20703054 and 21173249). This work is also supported by Synfuels CHINA. Co., Ltd.

References

[1] H. Schulz, Appl. Catal. A: Gen. 186 (1999) 3–12.
[2] D.S. Kalakkad, M.D. Shroff, S. Köhler, N. Jackson, A.K. Datye, Appl. Catal. A: Gen. 133 (1995) 335–350.
[3] K. Jothimurugesan, J.G. Goodwin Jr., S.K. Gangwal, J.J. Spivey, Catal. Today 58 (2000) 335–344.
[4] M.E. Dry, G.J. Oosthuizen, J. Catal. 11 (1968) 18–24.
[5] D.B. Bukur, X. Lang, D. Mukesh, W.H. Zimmerman, M.P. Rosynek, C. Li, Ind. Eng. Chem. Res. 29 (1990) 1588–1599.
[6] K. Sudsakorn, J.G. Goodwin Jr., K. Jothimurugesan, A.A. Adeyiga, Ind. Eng. Chem. Res. 40 (2001) 4778–4784.
[7] R. Zhao, J.G. Goodwin Jr., K. Jothimurugesan, S.K. Gangwal, J.J. Spivey, Ind. Eng. Chem. Res. 40 (2001) 1065–1075.
[8] R. O'Brien, L.G. Xu, S.Q. Bao, A. Raje, B.H. Davis, Appl. Catal. A: Gen. 196 (2000) 173–178.
[9] A.F.H. Wielers, A.J.H.M. Kock, C.E.C.A. Hop, J.W. Geus, A.M. van der Kraan, J. Catal. 117 (1989) 1–18.
[10] Y. Yang, H.W. Xiang, L. Tian, H. Wang, C.H. Zhang, Z.C. Tao, Y.Y. Xu, B. Zhong, Y.W. Li, Appl. Catal. A: Gen. 284 (2005) 105–122.
[11] C.H. Zhang, Y. Yang, B.T. Teng, T.Z. Li, H.Y. Zheng, H.W. Xiang, Y.W. Li, J. Catal. 237 (2006) 405–415.
[12] C.H. Zhang, H.J. Wan, Y. Yang, H.W. Xiang, Y.W. Li, Catal. Commun. 7 (2006) 733–738.
[13] D.A. Donatti, A.I. Ruiz, D.R. Vollet, Ultrason. Sonochem. 9 (2002) 133–138.
[14] L.B. Wu, D. Cao, Y. Huang, B.G. Li, Polymer 49 (2008) 742–748.
[15] N. Lohitharn, J.G. Goodwin Jr., E. Lotero, J. Catal. 255 (2008) 104–113.
[16] H.J. Wan, B.S. Wu, C.H. Zhang, H.W. Xiang, Y.W. Li, B.F. Xu, F. Yi, Catal. Commun. 8 (2007) 1538–1545.
[17] B. Kolk, I. Albers, R.I.R. Leith, M.G. Howden, Appl. Catal. 37 (1988) 57–74.
[18] F.R. van der Berg, M.W.J. Craj, A.M. van der Kraan, J.W. Geus, Appl. Catal. A: Gen. 251 (2003) 347–357.
[19] H. Dlamini, T. Motjope, G. Joorst, G. ter Stege, M. Mdleleni, Catal. Lett. 78 (2002) 201–207.
[20] E. de Smit, A.M. Bealea, S. Nikitenko, B.M. Weckhuysen, J. Catal. 262 (2009) 244–256.
[21] F.J. Berry, S. Skinner, M.F. Thomas, J. Phys.: Condens. Matter 10 (1998) 215–220.
[22] F.X. Redl, C.T. Black, G.C. Papaefthymiou, R.L. Sandstrom, M. Yin, H. Zeng, C.B. Murray, S.P. O'Brien, J. Am. Chem. Soc. 126 (2004) 14583–14599.
[23] J.F. Bengoa, A.M. Alvarez, M.V. Cagnoli, N.G. Gallegos, S.G. Marchetti, Appl. Catal. A: Gen. 325 (2007) 68–75.
[24] S.C. Lin, J. Phillips, J. Appl. Phys. 58 (1985) 1943–1949.
[25] S.S. Hafner, J. Stanek, M. Stanek, J. Phys. Chem. Solids 51 (1990) 203–208.
[26] W.S. Ning, N. Koizumi, H. Chang, T. Mochizuki, T. Itoh, M. Yamada, Appl. Catal. A: Gen. 312 (2006) 35–44.
[27] H.L. Wang, Y. Yang, J. Xu, H. Wang, M.Y. Ding, Y.W. Li, J. Mol. Catal. A: Chem. 326 (2010) 29–40.
[28] W.J. Hou, B.S. Wu, X.T. An, Z. Li, Z.C. Tao, H.Y. Zheng, H.W. Xiang, Y.W. Li, Catal. Lett. 119 (2007) 353–360.
[29] F. Arena, G. Gatti, G. Martra, S. Coluccia, L. Stievano, L. Spadaro, P. Famulari, A. Parmaliana, J. Catal. 231 (2005) 365–380.
[30] X. Gao, J. Shen, Y. Hsia, Y. Chen, J. Chem. Soc. Faraday. Trans. 89 (1993) 1079–1084.
[31] M.L. Burke, R.J. Madix, Surf. Sci. 237 (1990) 20–34.
[32] P.B. Merrill, R.J. Madix, Surf. Sci. 347 (1996) 249–264.
[33] G.D. Weatherbee, J.L. Rankin, C.H. Bartholomew, Appl. Catal. 11 (1984) 73–84.
[34] F.S. Modica, J.T. Miller, B.L. Meyers, D.C. Koningsberger, Catal. Today 21 (1994) 37–48.
[35] P. Braos-García, C. García-Sancho, A. Infantes-Molina, E. Rodríguez-Castellón, A. Jiménez-López, Appl. Catal. A: Gen. 381 (2010) 132–144.
[36] J.L. Rankin, C.H. Bartholomew, J. Catal. 100 (1986) 526–532.
[37] B.S. Clausen, S. Mørup, H. Topsøe, Surf. Sci. 106 (1981) 438–443.
[38] J. Benziger, R.J. Madix, Surf. Sci. 94 (1980) 119–153.
[39] U. Seip, M.C. Tsai, K. Christmann, J. Kippers, G. Ertl, Surf. Sci. 139 (1984) 29–42.
[40] D.W. Moon, S.L. Bernasek, J.P. Lu, J.L. Gland, D.J. Dwyer, Surf. Sci. 184 (1987) 90–108.
[41] N. Sirimanothan, H.H. Hamdeh, Y. Zhang, B.H. Davis, Catal. Lett. 82 (2002) 181–191.
[42] H.J. Jung, P.L. Walker Jr., M.A. Vannice, J. Catal. 75 (1982) 416–422.
[43] V.K. Jones, L.R. Neubauer, C.H. Bartholomew, J. Phys. Chem. 90 (1986) 4832–4839.
[44] S.D. Qin, C.H. Zhang, J. Xu, H.W. Xiang, Y.H. Li, Appl. Catal. A: Gen. 392 (2011) 118–126.